



High-resolution spectroscopy and preliminary global analysis of C–H stretching vibrations of C₂H₄ in the 3000 and 6000 cm⁻¹ regions

Marcos Loroño, Vincent Boudon, Michel Loete, Maud Rotger, Marie-Thérèse Bourgeois, Kévin Didriche, Michel Herman, V. A. Kapitanov, Yu.V. Ponomarev, A. A. Solodov, et al.

► To cite this version:

Marcos Loroño, Vincent Boudon, Michel Loete, Maud Rotger, Marie-Thérèse Bourgeois, et al.. High-resolution spectroscopy and preliminary global analysis of C–H stretching vibrations of C₂H₄ in the 3000 and 6000 cm⁻¹ regions. *Journal of Quantitative Spectroscopy and Radiative Transfer*, 2010, 111, pp.2151-2159. hal-00482394

HAL Id: hal-00482394

<https://hal.science/hal-00482394>

Submitted on 10 May 2010

HAL is a multi-disciplinary open access archive for the deposit and dissemination of scientific research documents, whether they are published or not. The documents may come from teaching and research institutions in France or abroad, or from public or private research centers.

L'archive ouverte pluridisciplinaire **HAL**, est destinée au dépôt et à la diffusion de documents scientifiques de niveau recherche, publiés ou non, émanant des établissements d'enseignement et de recherche français ou étrangers, des laboratoires publics ou privés.

High-resolution spectroscopy and preliminary global analysis of C–H stretching vibrations of C₂H₄ in the 3000 and 6000 cm⁻¹ regions

M. A. Loroño Gonzalez

Department of Chemistry, Universidad de Oriente, Cumaná 6101, Estado Sucre, Venezuela

V. Boudon*, M. Loëte

Laboratoire Interdisciplinaire Carnot de Bourgogne, UMR 5209 CNRS-Université de Bourgogne, 9. Av. A. Savary, BP 47870, F-21078 Dijon Cedex, France

M. Rotger, M.-T. Bourgeois

Groupe de Spectrométrie Moléculaire et Atmosphérique (GSMA), CNRS UMR 6089, Moulin de la Housse, BP 1039, Cases 16-17, F-51687 Reims Cedex 2, France

K. Didriche, M. Herman

Laboratoire de Chimie quantique et Photophysique, CP160/09, Faculté des Sciences, Université Libre de Bruxelles, 50 ave. Roosevelt, B-1050, Brussels, Belgium

V. A. Kapitanov, Yu. N. Ponomarev, A. A. Solodov

Laboratory of Atmospheric Absorption Spectroscopy, V.E. Zuev Institute of Atmospheric Optics SB RAS, 1, Zuev Square, Tomsk, 634921, Russian Federation

A. M. Solodov, T. M. Petrova

Laboratory of Molecular Spectroscopy, V.E. Zuev Institute of Atmospheric Optics SB RAS, 1, Zuev Square, Tomsk, 634921, Russian Federation

Abstract

Ethylene (ethene, H₂C=CH₂) is a naturally occurring compound in ambient air that affects atmospheric chemistry and global climate. The C₂H₄ spectrum is available in databases only for the 1000 and 3000 cm⁻¹ ranges.

In this work, the ethylene absorption spectrum was measured in the 6030–6250 cm⁻¹ range with the use of a high resolution Bruker IFS 125HR Fourier-spectrometer and a two-channel opto-acoustic spectrometer with a diode laser.

*To whom correspondence should be addressed.
E-mail: Vincent.Boudon@u-bourgogne.fr.
Fax : +33 3 80 39 59 17

As a secondary standard of wavelengths, the methane absorption spectrum was used in both cases.

A preliminary analysis was realized thanks to the tensorial formalism developed by the Dijon group that is implemented in the XTDS software package [Ch. Wenger, V. Boudon, M. Rotger, J.-P. Champion and M. Sanzharov, *J. Mol. Spectrosc.*, **251**, 102–113 (2008).]. We considered the two combination bands $\nu_5 + \nu_9$ and $\nu_5 + \nu_{11}$ as an interacting dyad. Parameters for the ν_9/ν_{11} dyad were fitted simultaneously from a re-analysis of previously recorded supersonic expansion jet FTIR data, while parameters for the $\nu_5 = 1$ Raman level were taken from literature. More than 600 lines could be assigned in the 6030–6250 cm^{-1} region (and also 682 in the 2950–3150 cm^{-1} region) and effective Hamiltonian parameters were fitted, including Coriolis interaction parameters. The dyad features are globally quite well reproduced, even if there are still problems at high J values.

Keywords: Ethylene; Infrared absorption; Diode laser spectroscopy; Fourier transform spectroscopy; Earth and planetary atmospheres

1. Introduction

Ethylene is a natural component of atmospheric air, which actively participates in various chemical processes. As it is also a hormone for the growth of plants, its influence on the plant biochemistry, ecology, metabolism of human beings and animals is of significant interest for several areas of research [1, 2]. Because of its very high activity relative with hydroxyl radical (OH), ethylene affects the ozone concentration in the atmosphere. All these factors make it an important contaminant and, therefore, the monitoring of its atmospheric concentration, sources, and sinks is of great importance. Moreover, ethylene is also present in the atmosphere of giant planets like Jupiter [3] or Neptune [4, 5, 6, 7, 8] and of Titan [9, 10, 11].

The background content of ethylene in the atmosphere is within 10–50 ppb. The global ethylene emission into the atmosphere is roughly estimated as 18–45 millions of tons per year; among them 74% are due to natural sources and 26% are due to anthropogenic sources, respectively; the major ethylene sink is determined by reactions with the OH radical (85%) and with ozone (15%) [12].

Infrared (IR) laser methods such as photo-acoustic (PAS), cavity ring down (CRDS) and cavity enhanced absorption (CEAS) spectroscopies are today available for remote sensing. They can lead to multi-component detection with sensitivities similar to those of more conventional techniques such as mass spectrometry and gas chromatography. They rely on cheap and reliable diode lasers today available in the 1.5–1.8 μm spectral range. Lots of relevant molecules can therefore be detected from their combination and overtones absorption bands, such as H_2O , CO_2 , CH_4 , CO , C_2H_4 . The monitoring of the concentration of these molecules necessitates accurate information about their absorption spectra: line-center positions, line intensities, spectral line shape contours, line broadening

coefficients and line-center shifts. Present data bases provide information on absorption spectra of H₂O, CO₂, CH₄, CO in 1.65 μm region which is, however incomplete, regarding pressure shifts in particular, and sometimes incorrect.

The C₂H₄ spectrum available in databases is limited to few spectral ranges around 1000 and 3000 cm⁻¹. As a matter of fact, the literature data on the ethylene absorption spectrum are only reported in reviews and therefore not optimally accessible. In the 5900–6400 cm⁻¹ range [13] the ethylene absorption spectrum has been recorded at a low resolution (5 cm⁻¹). The ethylene Fourier Transform (FT) spectrum at a resolution of 0.02 cm⁻¹ in a supersonic flow is reported in [14] and at a resolution of 0.015 cm⁻¹ in the 6070–6230 cm⁻¹ range in [15], along with opto-acoustic and opto-thermal spectra in the 6147–6170 cm⁻¹ range in a collimated beam. The systematic error in the determination of line-centers in [15] is of the order of 0.004 cm⁻¹. Higher resolution was achieved in very limited spectral ranges in [16] (6154–6159 cm⁻¹), [17] (6149.7–6150.48 cm⁻¹), and [16] (6157.55–6158.25 cm⁻¹). Earlier, the authors of [18] presented the ethylene absorption spectrum in the 6035–6210 cm⁻¹ range, recorded with the use of a two-channel PA spectrometer combined with a diode laser, characterized by a threshold absorption sensitivity of 1.4×10^{-6} cm⁻¹. The comparison of the ethylene absorption spectrum [18] with data presented in [15, 16, 17, 19] has shown a discrepancy in line-center positions from 0.005 cm⁻¹ [17] to 0.32 cm⁻¹ [16]. The ethylene absorption cross-sections were reported in [17], only.

In this work, the ethylene absorption spectrum was recorded in the 6030–6250 cm⁻¹ range using a high resolution Bruker IFS 125HR FT spectrometer (Russia, Tomsk, IAO SB RAS) and a two-channel photo-acoustic spectrometer with a diode laser (PAS DL). The methane absorption spectrum [20, 21] was used in both cases as a reference spectrum to validate the absolute wavenumber measurements. The use of methane lines as secondary standard of wavenumbers ensures the consistency of the line position measurements in the FT and PA spectra.

These data were used to assign the strongest bands in the 6030–6250 cm⁻¹ spectral range, *i.e.* $\nu_5 + \nu_9$ and $\nu_5 + \nu_{11}$. Their analysis was performed by considering them as a dyad. It was helped by previous information on the ν_9 and ν_{11} bands resulting from slit-jet expansion FTIR spectra recorded in the 2950–3150 cm⁻¹ region [22]. We actually performed a simultaneous fit of both regions (ν_9/ν_{11} stretching dyad around 3000 cm⁻¹ and $\nu_5 + \nu_9/\nu_5 + \nu_{11}$ dyad around 6100 cm⁻¹), also using literature Raman results on ν_5 [23].

The experiments, model and results, are presented in sections 2, 3 and 4, respectively, before concluding.

2. Experimental details

2.1. Jet-cooled FTIR spectra in Brussels

For the 3 μm region, we used a supersonic expansion jet spectrum previously recorded in the 2500–3500 cm⁻¹ region [22]. We just briefly recall here the experimental conditions.

We used a high-resolution FT interferometer Bruker IFS120 HR working at 0.01 cm^{-1} resolution coupled to a supersonic expansion experiment. The expansion was produced through a 15 cm long and 20 micron wide stainless steel slit. We used a 1:9 mixture of ethylene and argon, with 1380 and 0.5 hPa stagnation and residual pressure conditions, respectively. The rotational temperature was estimated to 36 K from the relative intensity of the vibration-rotation lines. Line positions were measured using water lines as references, from [24]. More complete experimental conditions are provided in [22] and [25]. At the time only preliminary constants were obtained from spectral analysis. Hot bands could be identified from a comparison between spectra recorded with and without heating the slit.

2.2. High-resolution Fourier transform spectrometer in Tomsk

Measurements of the ethylene absorption spectrum were conducted with the use of a high-resolution FT spectrometer Bruker IFS 125HR. The internal tungsten light source was selected; the radiation was recorded with an InSb detector, cooled at liquid nitrogen temperature. To measure the spectra, we have built a quartz cell 20 cm in length and 20 mm in diameter; its windows were made of CaF_2 . The cell was located in the spectrometer sample chamber. The FTS was pumped out up to a residual pressure of 0.015 Torr with a forevacuum pump, which significantly decreased the effect of atmospheric gases on the measured absorptions.

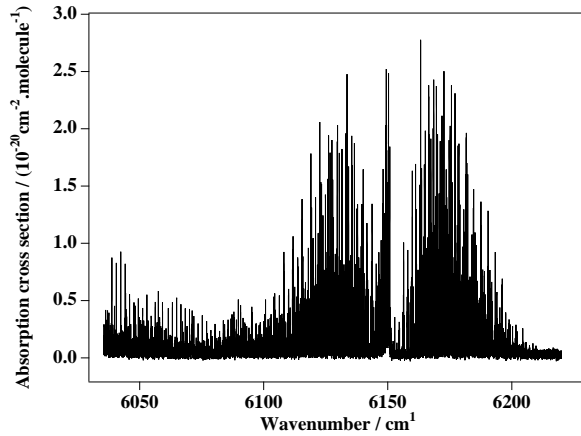


Figure 1: General view of the ethylene absorption spectrum recorded with a FT spectrometer.

The ethylene absorption spectrum was recorded at room temperature and at a pressure of 19 Torr with a spectral resolution of 0.005 cm^{-1} and an optical path length of 20 cm. Ethylene with 99.9% stated purity was used. The pressure was measured using the DVR-5 pressure gauge with an accuracy of less than 1 Torr. The frequency scale was calibrated using methane rovibrational lines belonging to the $2\nu_3$ band [20, 21].

To eliminate the temperature and pressure instabilities, which appeared just after filling the cell with the gas, measurements were conducted few hours after the filling. The signal-to-noise ratio (expressed as the maximum signal amplitude divided by twice the RMS noise amplitude) was about of 700. It was obtained by the coaddition of 1600 interferograms.

Figure 1 presents the record of the frequency-calibrated ethylene FTS spectrum within the $6030\text{--}6210\text{ cm}^{-1}$ range.

2.3. The two-channel OA spectrometer with TDL in Tomsk

The ethylene absorption photo-acoustic (PA) spectrum was recorded by the two-channel laser spectrometer. It includes a narrow-band tunable diode laser (TDL) with a controller, two opto-acoustic (OA) detectors, and the spectrometers microcontroller. A specificity of the PA spectrometer is the simultaneous recording of two spectra of different gases and mixtures under different experimental conditions. In our measurements, one PA detector (PAD) was filled the mixture of ethylene and nitrogen and the second PAD with pure CH_4 at a pressure of 5 or 7 Torr. The reference CH_4 line positions were used for calibrating the TDL radiation wavelength. Basic parameters of the spectrometer are presented in Table 1. The spectrometer scheme and measurement procedure are

Table 1: Specifications of the OA spectrometer.

Parameter	Value / cm^{-1}
Spectral interval	6020–6300
Spectral resolution	0.00033
Threshold sensitivity	0.4×10^{-6}

presented in more details in [26].

The TEC-100 semiconductor laser with an outer cavity (Sacher Laser Technik) generates the continuous single-frequency radiation within $6020\text{--}6300\text{ cm}^{-1}$ at a radiation spectrum width not exceeding $\sim 10\text{ MHz}$ and an output power of $0.003\text{--}0.01\text{ W}$. The radiation power is controlled with a built-in photodiode and is modulated with a variable frequency optical chopper, Model 300C, SCITEC INSTRUMENTS [27].

The laser radiation frequency is controlled through a diffraction grating. The grating is first rotated manually using a micro-screw to reach a desired wavenlength range. It can then be smoothly tuned, without mode jump, over 3 cm^{-1} using a piezoceramic device. This fine control is achieved using an electric signal produced from a 12-digit Digital-to-Analog Converter (DAC), which varies the piezoceramic voltage between zero and 100 V following a given program. The minimal variation step is $\sim 0.024\text{ V}$, which corresponds to a step of $\sim 22\text{ MHz}$ (0.00073 cm^{-1}) of the laser radiation frequency tuning.

Measurements and the control for setting laser radiation to a given initial wavelength are made with a wavelength meter of WS-7 117 IR type, produced

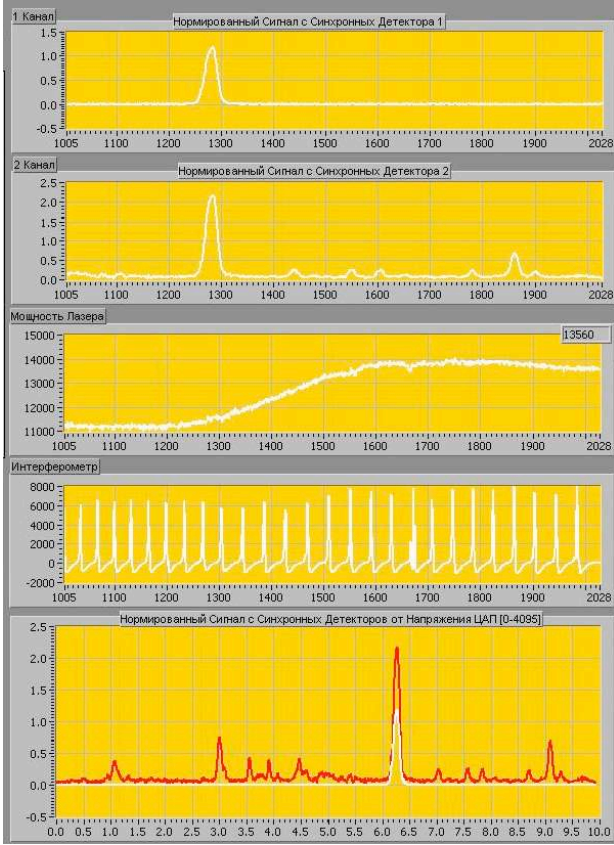


Figure 2: Menu of controlling and taking information from the two-channel spectrometer. See text for the description of the different traces.

by the Angstrom Company [28]. The absolute error of the initial wavelength measurements ($\Delta\lambda/\lambda$) does not exceed a value of 10^{-6} .

The control for the laser radiation frequency tuning in the program-controlled mode is performed with the use of the Fabry-Pérot standard (IT-28-30 with a base of 10 cm and a spectral dispersion range of 0.05 cm^{-1}). To eliminate the effect of jumps of the atmospheric air pressure on the value of the spectral dispersion range, the Fabry-Pérot etalon is located in a pressure-tight housing, filled with dry nitrogen at atmospheric pressure.

We used PA detectors (PAD) based on the differential Helmholtz resonator (DHR) [26]. This resonator has a remarkable peculiarity: acoustic oscillations in DHR cells at the resonance frequency are in anti-phase. Microphones, located in the cells, allow recording the difference between acoustic signals; therewith, the useful signal becomes duplicated, while the in-phase outer acoustic noise decreases by 1–2 orders of magnitude. The home-made DHR with two capillaries is symmetric and significantly decreases the noise level, even under gas flow con-

ditions. As the gas goes through the two DHR cells, the in-phase acoustic noise is generated in each of them and then removed using a differential amplifier. The threshold sensitivity of the DHR is $1 \times 10^{-9} \text{ cm}^{-1} \text{ Hz}^{-1/2} \text{ W}$.

A specially designed controller is used in order to automate measurements and to increase the accuracy and sensitivity. The 16-bit ADC ADS8725 (Texas Instruments) was incorporated into the controller for high-precision conversion of signals into digits from DHR microphones and from the laser power meter photodiode. To increase the device sensitivity, signals from both DHRs were detected synchronously in the computerized mode.

There is an analog output in the controller of the signal which is required for scanning operation. The device can be operated in the amplitude mode and in the signal derivative measuring mode. This derivative is achieved from two signals: the retuning voltage and the saw-tooth voltage of the laser beam modulation frequency. The management by the controller is realized through a serial port.

The controller intrinsic software is written in the Assembler language of microcontrollers of the AVR architecture. The calibrating and service software is written inside the LabVIEW 5.0 package medium and operates under Windows-XP, Windows-2000, and Windows-98 operation media. The on-screen user menu is presented in Figure 2.

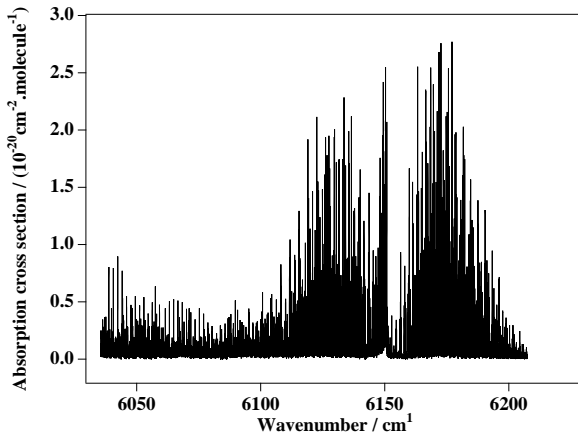


Figure 3: Ethylene PA absorption spectrum.

The two first windows of the menu represent signal amplitudes of DHR with the pure methane and with the mixture of ethylene and broadening gas (nitrogen), respectively. The middle window shows the value of the laser radiation power, and the next one – the Fabry-Pérot interferometer transmission. The bottom window shows the laser-power-normalized signals from both DHRs. The panel of the control for laser parameters, the synchronous detector, and the input of initial parameters, is to the left.

As previously mentioned, the smooth computer-controlled tuning of the TDL

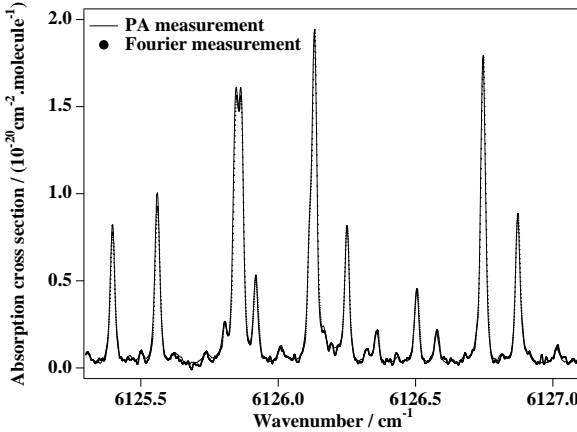


Figure 4: Comparison of ethylene absorption spectra within the $6125.3\text{--}6127.3\text{ cm}^{-1}$ range recorded with PA and FT spectrometers.

radiation frequency is possible only in a narrow spectral range of about 3 cm^{-1} . A piecewise continuous mode is then required to achieve recording over a selected wavelength range. To avoid troubles when concatenating the spectra, a reference line should appear in each fragment. The ethylene absorption spectrum was recorded simultaneously with reference methane lines in each narrow spectral range independently recorded. Ref. [29] was used for estimation of methane line positions.

Line center positions were estimated from the fitting of the recorded spectrum to the theoretical one. The accuracy is estimated to be between 0.0005 cm^{-1} for isolated lines and 0.004 cm^{-1} for strongly overlapped lines.

To increase the PAD sensitivity, measurements of the ethylene absorption spectrum were conducted for a mixture ethylene:nitrogen in the ratio 1:70 at a total pressure of 31 Torr (that is, a C_2H_4 pressure of 0.44 Torr) and a temperature of 293 K. The PAD calibration method and the estimation of the ethylene absorption cross-section are given in detail in [18].

Figure 3 shows the general view of the PA absorption ethylene spectrum.

The recorded spectrum exhibits a complex structure, the absorption line density can reach more than 20 lines per inverse centimeter with a line FWHM of 0.01 cm^{-1} .

Line density significantly hinders the line position and intensity measurement procedure. We therefore first superposed the spectra recorded using FT and PA methods to estimate how well they concided throughout the range under study ($6030\text{--}6200\text{ cm}^{-1}$) demonstrating an error of about 0.0005 cm^{-1} . Figure 4 shows the comparison of spectra in one of the fragments.

3. Theoretical details

X_2Y_4 -type molecules like ethylene possess twelve normal modes of vibration [30]. The symmetry labeling of these modes as well as of rovibrational energy levels leads to considerable confusion in the literature. This problem is related to the different possibilities to attach the x , y and z axes to the molecule. One striking feature is that most papers use different axes attachments for vibrational and rotational levels. As a matter of fact, there are two commonly used conventions for vibrations, say the IUPAC and Herzberg axes conventions (see Figure 5). The Herzberg one is the most popular. However, when speaking about rotational levels, the so-called I^r representation is generally used. And this representation is in fact another way of attaching axes that corresponds to none of the two previous ones! We simply suggest adopting the axis attachment of the I^r representation for the whole rovibrational problem.

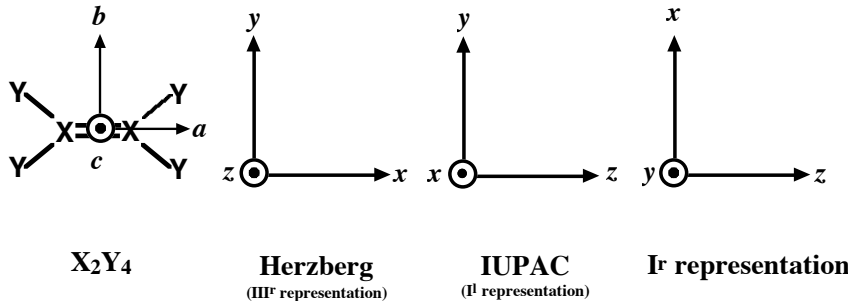


Figure 5: Various X_2Y_4 molecular axis frame conventions reported in the literature.

In this way, the 12 normal modes split up into five stretching modes, $\nu_1(A_g)$, $\nu_2(A_g)$, $\nu_5(B_{3g})$, $\nu_9(B_{2u})$ and $\nu_{11}(B_{1u})$, and seven bending modes, $\nu_3(A_g)$, $\nu_4(A_u)$, $\nu_6(B_{3g})$, $\nu_7(B_{3u})$, $\nu_8(B_{2g})$, $\nu_{10}(B_{2u})$ and $\nu_{12}(B_{1u})$, where the symbols between parentheses are the irreducible representations of the D_{2h} group. All g -parity bands are Raman active and all u -parity bands are infrared active, with the exception of ν_4 which is inactive. The modes are described in Table 2 and represented in [25].

We recently proposed a new tensorial formalism to analyze rovibrational spectra of D_{2h} asymmetric tops [31]. As already mentioned above, it is based on the work of Sartakov *et al.* [32]. It uses the formalism developed in Dijon for octahedral XY_6 molecules in the $O(3) \supset O_h$ group chain [33, 34, 35]. Such a formalism, together with vibrational extrapolation methods described for instance in [34, 35, 36], is implemented in the D_{2h} TDS program suite [37, 38].

In the following, the tensorial effective Hamiltonian and transition moment operators included in the model are outlined. Note that Γ ($= A_\tau$, $B_{1\tau}$, $B_{2\tau}$ or $B_{3\tau}$ with $\tau = g$ or u) denotes D_{2h} irreducible representations (irreps) and all operators are symmetrized in the $O(3) \supset D_{2h}$ group chain. The $O(3)$ standard

Table 2: The normal modes of ethylene in the I^r representation.

Mode	Wavenumber/cm ⁻¹	D_{2h} symmetry	Type
ν_1	3026	A_g	CH ₂ stretch
ν_2	1623	A_g	CC stretch
ν_3	1343.3	A_g	CH ₂ scissor
ν_4	1025.6	A_u	CH ₂ twist
ν_5	3083.4	B_{3g}	CH ₂ stretch
ν_6	1225.4	B_{3g}	CH ₂ rock
ν_7	948.8	B_{3u}	CH ₂ wag
ν_8	939.9	B_{2g}	CH ₂ wag
ν_9	3104.9	B_{2u}	CH ₂ stretch
ν_{10}	825.9	B_{2u}	CH ₂ rock
ν_{11}	2988.6	B_{1u}	CH ₂ stretch
ν_{12}	1442.4	B_{1u}	CH ₂ scissor

basis is oriented in the subgroup through the relation

$$|J, n\Gamma\rangle = \sum_M {}^{(J)}G_{n\Gamma}^M |J, M\rangle, \quad (1)$$

where n is the multiplicity index of the Γ irrep. The G coefficients are elements of the passage matrix from $O(3)$ into D_{2h} [31]. The tensorial operators are oriented in the same way.

Let us consider an X_2Y_4 molecule whose vibrational levels are grouped in a series of polyads designated by P_k ($k = 0, \dots, n, \dots$), P_0 being the ground state (GS). The X_2Y_4 Hamiltonian can be developed as a sum of operators specific to each polyad as

$$\mathcal{H} = \mathcal{H}_{\{P_0 \equiv \text{GS}\}} + \mathcal{H}_{\{P_1\}} + \dots + \mathcal{H}_{\{P_k\}} + \dots + \mathcal{H}_{\{P_{n-1}\}} + \mathcal{H}_{\{P_n\}} + \dots \quad (2)$$

The effective Hamiltonian for polyad P_n is obtained by projection in the corresponding subspace,

$$\begin{aligned} H^{< P_n >} &= P^{< P_n >} \mathcal{H} P^{< P_n >} \\ &= H_{\{\text{GS}\}}^{< P_n >} + H_{\{P_1\}}^{< P_n >} + \dots + H_{\{P_k\}}^{< P_n >} + \dots + H_{\{P_{n-1}\}}^{< P_n >} + H_{\{P_n\}}^{< P_n >}, \end{aligned} \quad (3)$$

the different terms being written as

$$\mathcal{H}_{\{P_k\}} = \sum_{\text{all indexes}} \beta t_{\{n_s\}\{m_s\}}^{\Omega(K, n\Gamma_r)\Gamma_1\Gamma_2\Gamma_v} \left(R^{\Omega(K, n\Gamma_r)} \otimes {}^\epsilon V_{\{n_s\}\{m_s\}}^{\Gamma_1\Gamma_2\Gamma_v} \right)^{(A_g)}. \quad (4)$$

In this equation, the $t_{\{n_s\}\{m_s\}}^{\Omega(K, n\Gamma_r)\Gamma_1\Gamma_2\Gamma_v}$ are the parameters to be determined. $R^{\Omega(K, n\Gamma_r)}$ and ${}^\epsilon V_{\{n_s\}\{m_s\}}^{\Gamma_1\Gamma_2\Gamma_v}$ are rotational and vibrational operators of respective

degree Ω (maximum degree in the rotational angular momentum components J_x , J_y and J_z) and Ω_v (degree in creation and annihilation operators). The order of each individual term is defined as $\Omega + \Omega_v - 2$. The construction of these operators is described in [34]. β is a numerical factor equal to $(-\sqrt{3}/4)^{\Omega/2}$ if $(K, n\Gamma_r) = (0, 0A_g)$ and 1 otherwise.

Such an Hamiltonian development scheme enables the treatment of any polyad system. In this work, the following four effective Hamiltonians have been used:

- The Ground State (polyad P_0) effective Hamiltonian

$$H^{<P_0>} = H_{\{P_0\}}^{<P_0>}. \quad (5)$$

- The ν_5 (polyad P_1) effective Hamiltonian

$$H^{<P_1>} = H_{\{P_0\}}^{<P_1>} + H_{\{P_1\}}^{<P_1>}. \quad (6)$$

- The ν_9/ν_{11} (polyad P_2) effective Hamiltonian

$$H^{<P_2>} = H_{\{P_0\}}^{<P_2>} + H_{\{P_1\}}^{<P_2>} + H_{\{P_2\}}^{<P_2>}. \quad (7)$$

- The $\nu_5 + \nu_9/\nu_5 + \nu_{11}$ (polyad P_3) effective Hamiltonian

$$H^{<P_3>} = H_{\{P_0\}}^{<P_3>} + H_{\{P_1\}}^{<P_3>} + H_{\{P_2\}}^{<P_3>} + H_{\{P_3\}}^{<P_3>}. \quad (8)$$

It should be noticed that, although ν_5 lies in the same spectral region as ν_9 and ν_{11} , it is a Raman active vibrational level of g parity, which does not interact at all with the infrared active levels. It thus appeared more practical to put it into a separate polyad.

To derive rovibrational energies, the matrix elements of the Hamiltonian operator need to be calculated. They are obtained in the coupled basis

$$|[\Psi_r^{(J,nC_r)} \otimes \Psi_{\{v_i\}}^{(C_v)}]^{(C)}\rangle, \quad (9)$$

where $v_i = v_1 \dots v_{12}$ are the vibrational quantum numbers for the X_2Y_4 molecule, and C_v , C_r and C are the vibrational, rotational and ro-vibrational symmetries in D_{2h} , respectively. With such a formalism, all the rovibrational levels are described by (J, C, α) labels, where α is a numbering index for levels that have the same D_{2h} symmetry within a J block (J is the quantum number associated to the total angular momentum of the molecule). This labelling is related to our group chain choice, which is an orientation from $O(3)$ into the symmetry subgroup of the X_2Y_4 molecule. In this way, the usual (K_a, K_c) labels are hidden and related to α and the C symmetry. Thus, the K_a and K_c values do not appear explicitly in our labels and the $(\Delta K_a, \Delta K_c)$ nomenclature does not occur in our transition labels. Expressions of the matrix elements of the Hamiltonian operator are given in [31].

To calculate line intensities, the dipole moment operator (for absorption spectra) is expanded in a similar way, as detailed in [31] (see Eq. 58 to 61). As we do not consider here absolute intensities, this expansion is just taken up to the minimum possible order and we do not discuss this point any further.

4. Analysis

The analysis has been performed thanks to the XTDS software [39] that implements the $O(3) \supset D_{2h}$ tensorial formalism described briefly above [31, 37]. Line assignments were realized using the SPVIEW graphical interface [39].

As a first step, we started from ground state [22], ν_5 [23] (Raman band), ν_9 (C -type band) and ν_{11} [22] (A -type band) parameters taken from the literature. Parameters from these references are given for a A -reduction Watsonian Hamiltonian. We translated them into tensorial formalism parameters thanks to the formula given in [40]. Ground state and ν_5 parameters were kept as obtained in this way and fixed in the following.

As a second step, we started to perform an initial simulation of the 3000 cm^{-1} region (polyad P_2) using these parameters. This allowed us to assign 682 lines in the ν_9/ν_{11} stretching dyad from the FTIR supersonic expansion jet spectrum (see Section 2.1). It should be noticed that we did not use assignments for polyad P_2 from [22]; we reassigned the supersonic expansion jet completely. Because of different labels for levels and transitions (see previous section), the detailed comparison of our new assignments with those of [22] has not been attempted.

Table 3: Fit statistics for ethylene data.

Polyad	Number of data	J_{\max}	$d_{\text{RMS}}/\text{cm}^{-1}$	Fitted parameters
ν_9/ν_{11}	682	32	0.010	40
$\nu_5 + \nu_9/\nu_5 + \nu_{11}$	608	27	0.026	20

The same initial parameter set allowed the 6000 cm^{-1} region (polyad P_3) to be simulated, thanks to the vibrational extrapolation scheme explained in the previous section. We used the PA spectrum as experimental data (see Section 2.3). By changing by hand the anharmonicity parameters (*i.e.* by moving the $\nu_5 + \nu_9$ (A -type band) and $\nu_5 + \nu_{11}$ (C -type band) band centers so that they would match with the values that can be estimated from the experimental spectrum), it was possible to obtain a reasonable simulation and then to perform assignments. After several iterations, we could finally identify 608 spectral lines in the P_3 region.

Table 3 summarizes the statistics for the final fit. As explained in the previous section, our energy level and transition labels do not include the usual K_a and K_c quantum numbers; retrieving their maximum values is quite complex to perform and has not been attempted here. We determined 40 parameters for polyad P_2 , including four Coriolis interaction parameters between ν_9 and ν_{11} and 20 parameters for polyad P_3 , including two Coriolis interaction parameters between $\nu_5 + \nu_9$ and $\nu_5 + \nu_{11}$. Figure 6 displays the calculated and observed reduced energy levels as defined by:

$$\tilde{\nu}_{\text{red}} = \tilde{\nu} - \sum_{\Omega} t_{\{\text{GS}\}\{\text{GS}\}}^{\Omega(0,0A_1)A_1A_1A_1} (J(J+1))^{\Omega/2} \quad (10)$$

(this corresponds to the subtraction of scalar terms). This shows how the energy levels are “sampled” by the observed transitions. The ratio of the number of observed levels over the number of fitted parameters is *ca.* 7 for polyad P_2 and *ca.* 17 for polyad P_3 .

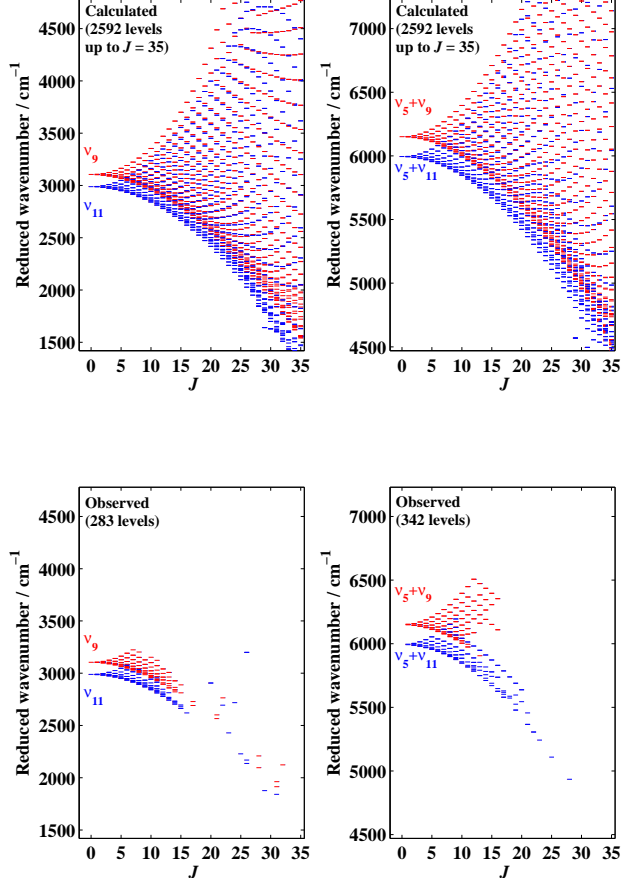


Figure 6: Calculated (top) and observed (bottom) reduced energy levels (see text) for polyads P_2 (left) and P_3 (right). Observed levels are levels reached by assigned transitions.

Values of the parameters are given in Table A.1 in the Appendix. It should be noticed from this table that one parameter of the ν_9 band that could not be fitted (because of a 100 % correlation with other parameters) was fixed to a particular values that gives the lowest root means square deviation (fixing it to 0 corresponds more or less to the so-called A-reduction of Watson [41, 40], but gives a somewhat degraded fit).

Although the root mean square deviations are still high compared to usual high-resolution spectroscopy standards, the agreement of this preliminary analysis is quite satisfactory. The deviation for polyad P_2 is of the same order of

magnitude as the resolution of the jet-FTIR spectrum used here. The deviation for polyad P_3 is somewhat higher (because of an even higher number of neglected resonances), for a lower maximum J value, but still within reasonable limits.

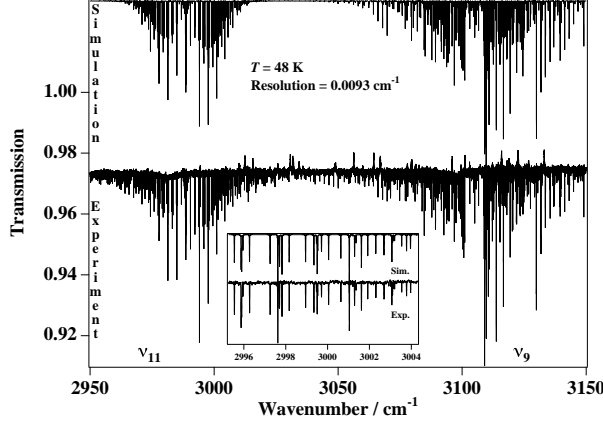


Figure 7: Overview of the experimental FT spectrum of ethylene in the 3000 cm^{-1} region compared to the simulation. The insert shows a portion of the ν_{11} band.

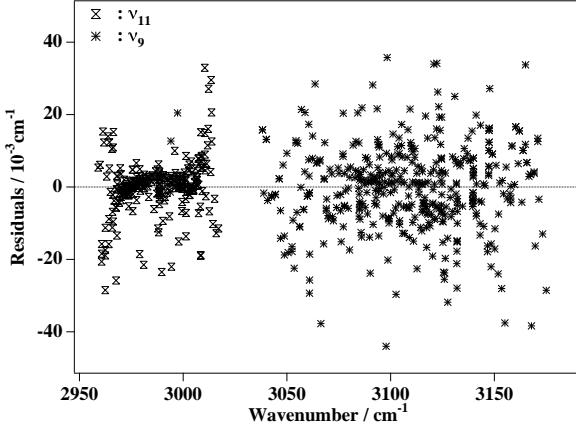


Figure 8: Residuals of the fit in the 3000 cm^{-1} spectral range of ethylene, as a function of wavenumber.

What should be kept in mind is that we have used here a crude approximation by considering P_2 and P_3 as isolated dyads. Both are in fact just parts of more complex polyads with many interacting bands in each case. The present work should thus be viewed as a preliminary approach for a global fit of both spectral regions using a simple polyad scheme and the tensorial formalism method. As a matter of fact, previous analyses give some better results for each

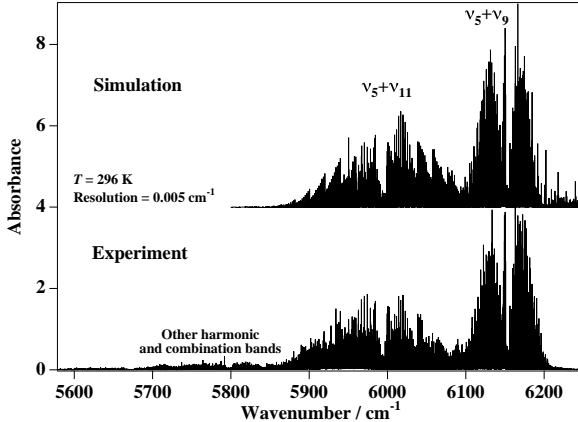


Figure 9: Overview of the experimental and simulated spectra of ethylene in the 6000 cm^{-1} region.

region when considered separately. Reference [32] uses very high resolution laser spectroscopy data to investigate the $3\text{ }\mu\text{m}$ region; the fit includes 34 vibrational states. In the $1.6\text{ }\mu\text{m}$ region, the authors of [42] include several dark states to obtain a satisfying fit. It is thus neither easy nor really relevant to perform a detailed comparison with the present study that has a different aim, as stated above. Table 4 just compares the band centers found in this work with those from the two previously cited references, showing a good agreement. In Appendix B, we also compare the rovibrational levels that were observed in the present polyad P_2 by Sartakov *et al.* [32] with those resulting from the present fit. There is a global good consistency with previous analyses for the literature, although some differences are observed. Again, this is mainly due to the simple polyad scheme used here, which does not aim to reach a state-of-the-art level.

Table 4: Band centers resulting from the present fit, compared to literature values.

Band	This work	Ref. [32]	Ref. [42]
ν_9	3104.8744	3104.887	
ν_{11}	2988.6347	2988.643	
$\nu_5 + \nu_9$	6150.9927		6150.9810
$\nu_5 + \nu_{11}$	5994.7980		5994.7854

Figure 7 shows a comparison between observed and simulated spectra involving polyad P_2 (3000 cm^{-1} region) and Figure 8 displays the fit residuals.

Figure 9 shows a comparison between experiment and simulation of polyad P_3 (6000 cm^{-1} region), with some detailed view into the $\nu_5 + \nu_9$ and $\nu_5 + \nu_{11}$ bands given in Figures 10 and 11, respectively. Figure 12 displays the fit

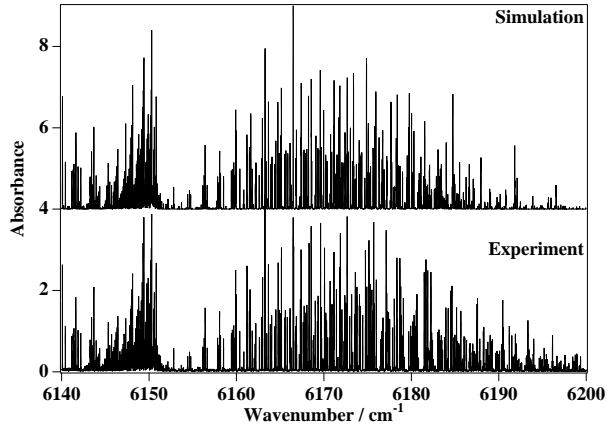


Figure 10: Detail in the $\nu_5 + \nu_9$ band of ethylene compared to the simulation.

residuals in this case.

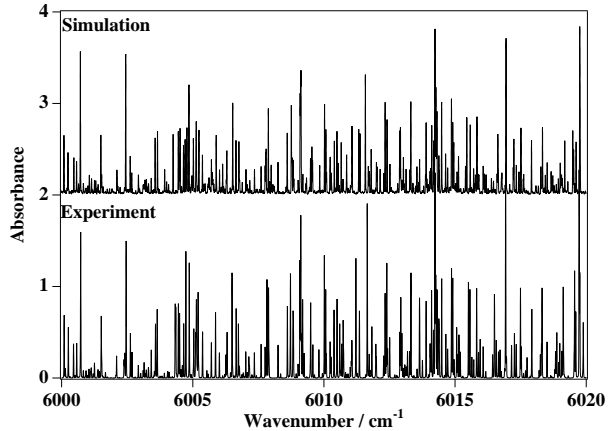


Figure 11: Detail in the $\nu_5 + \nu_{11}$ band of ethylene compared to the simulation.

5. Conclusion

We have performed a preliminary global analysis of the 3000 and 6000 cm^{-1} spectral regions of ethylene by considering only the ν_9 , ν_{11} , $\nu_5 + \nu_9$ and $\nu_5 + \nu_{11}$ bands and using the tensorial formalism model developed in the Dijon group. A high-resolution spectrum of the combination band region has been recorded for the first time in Tomsk. The results of the analysis are quite very satisfying. They are now included into the XTDS [39, 38] system that allows synthetic linelists and spectra to be calculated.

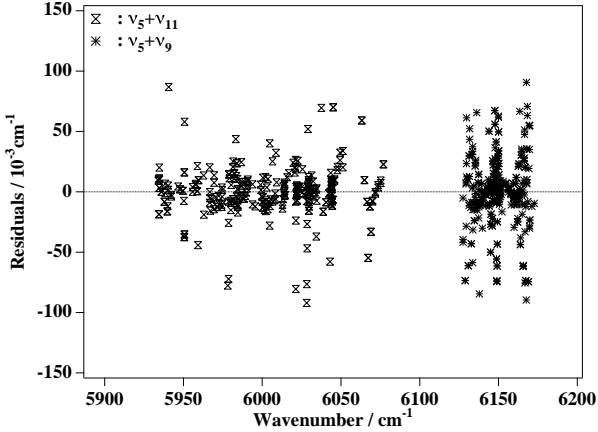


Figure 12: Residuals of the fit in the 6000 cm^{-1} spectral range of ethylene, as a function of wavenumber.

Of course, the model presented here does not pretend to reflect all the real couplings between rovibrational bands. The main purpose of this work is to demonstrate the use of tensorial formalism and vibrational extrapolation methods in the case of a simplified global analysis of ethylene C–H stretching modes. More generally, the C_2H_4 molecule is difficult to study because, starting from the very first fundamental bands (see for example [43]), the resonances coupling (like $\nu_4 \leftrightarrow \nu_7$, $\nu_4 \leftrightarrow \nu_{10}$, $\nu_{10} \leftrightarrow \nu_{12}$, ... etc) are very strong. Necessarily, this scheme of resonances is also present in the system of the $\nu_7 + \nu_{11} \leftrightarrow \nu_4 + \nu_{11}$, $\nu_4 + \nu_{11} \leftrightarrow \nu_{10} + \nu_{11}$, ... etc, excited states (see Ref. [44]). More or less it is “a copy” of the resonances observed for the fundamentals states. The present work describes the study of two dyads of interacting states, $\nu_9 \leftrightarrow \nu_{11}$ and $(\nu_5 + \nu_9 \leftrightarrow \nu_5 + \nu_{11})$. The main advantage of the theoretical model which is presented here is that, in principle, the informations on the parameters involved in the resonance coupling the energy levels from the first system of interacting states ($\nu_9 \leftrightarrow \nu_{11}$) are (at least partly) transferred to the overtones interacting bands ($\nu_5 + \nu_9 \leftrightarrow \nu_5 + \nu_{11}$). This major advantage of using the XTDS formalism will certainly be extremely useful when undertaking a more global study involving more vibrational states. Thus, the present paper is a first simple illustration of this.

The next natural steps in this work thus involve: 1) measuring and fitting absolute line intensities, which is essential for ethylene concentration retrievals, for instance and 2) considering more interacting bands in both polyads. Both points still require a lot of experimental and theoretical work to be achieved.

Acknowledgments

The contribution of the IAO SB RAS team is supported by the Russian Foundation for Basic Research (project 07-03-92210_a). VB and ML thank the

“Pôle de Sciences Planétaires” of Bourgogne Franche-Comté. VB, ML, MR and MTB acknowledge support from the LEFE-CHAT national program and the “SpecMo” GdR number 3152 of the CNRS. MR acknowledge support from the PNP national program and PHC Tournesol program handled by EGIDE. In Brussels this work was supported by the Fonds National de la Recherche Scientifique (F.R.S.-FNRS, contracts FRFC and IISN) and the “Action de Recherches Concertées de la Communauté française de Belgique”.

Appendix A. Effective Hamiltonian parameters

The following Table (A.1) gives the effective Hamiltonian parameters in the tensorial formalism notation (see for instance [36] for more details) and resulting from the global fit.

Table A.1: Effective Hamiltonian parameters for $^{12}\text{C}_2\text{H}_4$. The standard deviation of each parameter is given in parentheses, in the unit of the last two digits; parameters without standard deviation indicated are fixed.

Polyad	Order	$\Omega(K, nC)$	$\{s\}$	C_1	$\{s'\}$	C_2	Value / cm^{-1}
GS	0	2(0, 0A g)	000000000000A g	000000000000A g	2.23124666100		
GS	0	2(2, 0A g)	000000000000A g	000000000000A g	8.06317059500	$\times 10^{-2}$	
GS	0	2(2, 1A g)	000000000000A g	000000000000A g	-3.05790956300	$\times 10^{-2}$	
GS	2	4(0, 0A g)	000000000000A g	000000000000A g	-2.21791180000	$\times 10^{-5}$	
GS	2	4(2, 0A g)	000000000000A g	000000000000A g	7.45751178900	$\times 10^{-6}$	
GS	2	4(2, 1A g)	000000000000A g	000000000000A g	5.29991918800	$\times 10^{-7}$	
GS	2	4(4, 0A g)	000000000000A g	000000000000A g	-2.58488110100	$\times 10^{-6}$	
GS	2	4(4, 1A g)	000000000000A g	000000000000A g	-6.78019568700	$\times 10^{-7}$	
GS	2	4(4, 2A g)	000000000000A g	000000000000A g	0.0		
GS	4	6(0, 0A g)	000000000000A g	000000000000A g	8.67944507500	$\times 10^{-10}$	
GS	4	6(2, 0A g)	000000000000A g	000000000000A g	1.63171962800	$\times 10^{-10}$	
GS	4	6(2, 1A g)	000000000000A g	000000000000A g	2.59258189000	$\times 10^{-11}$	
GS	4	6(4, 0A g)	000000000000A g	000000000000A g	-1.04281366500	$\times 10^{-10}$	
GS	4	6(4, 1A g)	000000000000A g	000000000000A g	-6.23849869400	$\times 10^{-11}$	
GS	4	6(4, 2A g)	000000000000A g	000000000000A g	0.0		
GS	4	6(6, 0A g)	000000000000A g	000000000000A g	2.56880902600	$\times 10^{-11}$	
GS	4	6(6, 1A g)	000000000000A g	000000000000A g	2.97917925400	$\times 10^{-11}$	
GS	4	6(6, 2A g)	000000000000A g	000000000000A g	0.0		
GS	4	6(6, 3A g)	000000000000A g	000000000000A g	0.0		
v_5	0	0(0, 0A g)	000010000000B _{3g}	000010000000B _{3g}	3083.36000000000		
v_5	2	2(0, 0A g)	000010000000B _{3g}	000010000000B _{3g}	-9.80532800000	$\times 10^{-3}$	
v_5	2	2(2, 0A g)	000010000000B _{3g}	000010000000B _{3g}	-4.53053920000	$\times 10^{-3}$	
v_5	2	2(2, 1A g)	000010000000B _{3g}	000010000000B _{3g}	8.51157000000	$\times 10^{-5}$	
v_5	4	4(0, 0A g)	000010000000B _{3g}	000010000000B _{3g}	-3.08754867000	$\times 10^{-6}$	
v_5	4	4(2, 0A g)	000010000000B _{3g}	000010000000B _{3g}	1.70457178800	$\times 10^{-6}$	
v_5	4	4(2, 1A g)	000010000000B _{3g}	000010000000B _{3g}	5.29991918800	$\times 10^{-7}$	
v_5	4	4(4, 0A g)	000010000000B _{3g}	000010000000B _{3g}	-1.53731685000	$\times 10^{-7}$	
v_5	4	4(4, 1A g)	000010000000B _{3g}	000010000000B _{3g}	2.99256981800	$\times 10^{-6}$	
v_5	4	4(4, 2A g)	000010000000B _{3g}	000010000000B _{3g}	0.0		
v_5	6	6(0, 0A g)	000010000000B _{3g}	000010000000B _{3g}	8.67944507500	$\times 10^{-10}$	
v_5	6	6(2, 0A g)	000010000000B _{3g}	000010000000B _{3g}	1.63171962800	$\times 10^{-10}$	
v_5	6	6(2, 1A g)	000010000000B _{3g}	000010000000B _{3g}	2.59258189000	$\times 10^{-11}$	
v_5	6	6(4, 0A g)	000010000000B _{3g}	000010000000B _{3g}	-1.04281366500	$\times 10^{-10}$	
v_5	6	6(4, 1A g)	000010000000B _{3g}	000010000000B _{3g}	-6.23849869400	$\times 10^{-11}$	
v_5	6	6(4, 2A g)	000010000000B _{3g}	000010000000B _{3g}	0.0		
v_5	6	6(6, 0A g)	000010000000B _{3g}	000010000000B _{3g}	2.56880902600	$\times 10^{-11}$	
v_5	6	6(6, 1A g)	000010000000B _{3g}	000010000000B _{3g}	2.97917925400	$\times 10^{-11}$	
v_5	6	6(6, 2A g)	000010000000B _{3g}	000010000000B _{3g}	0.0		
v_5	6	6(6, 3A g)	000010000000B _{3g}	000010000000B _{3g}	0.0		
v_9/v_{11}	0	0(0, 0A g)	000000001000B _{2u}	000000001000B _{2u}	3104.87443(17)		
v_9/v_{11}	2	2(0, 0A g)	000000001000B _{2u}	000000001000B _{2u}	-6.451(13)	$\times 10^{-3}$	
v_9/v_{11}	2	2(2, 0A g)	000000001000B _{2u}	000000001000B _{2u}	-2.4808(60)	$\times 10^{-3}$	
v_9/v_{11}	2	2(2, 1A g)	000000001000B _{2u}	000000001000B _{2u}	1.1469(29)	$\times 10^{-3}$	
v_9/v_{11}	4	4(0, 0A g)	000000001000B _{2u}	000000001000B _{2u}	-5.363(34)	$\times 10^{-5}$	
v_9/v_{11}	4	4(2, 0A g)	000000001000B _{2u}	000000001000B _{2u}	2.9860(95)	$\times 10^{-5}$	
v_9/v_{11}	4	4(2, 1A g)	000000001000B _{2u}	000000001000B _{2u}	2.10628(92)	$\times 10^{-4}$	
v_9/v_{11}	4	4(4, 0A g)	000000001000B _{2u}	000000001000B _{2u}	-2.343(27)	$\times 10^{-6}$	
v_9/v_{11}	4	4(4, 1A g)	000000001000B _{2u}	000000001000B _{2u}	-3.2306(14)	$\times 10^{-4}$	
v_9/v_{11}	4	4(4, 2A g)	000000001000B _{2u}	000000001000B _{2u}	-1.08500000000	$\times 10^{-5}$	
v_9/v_{11}	6	6(0, 0A g)	000000001000B _{2u}	000000001000B _{2u}	5.071(28)	$\times 10^{-7}$	
v_9/v_{11}	6	6(2, 0A g)	000000001000B _{2u}	000000001000B _{2u}	4.428(46)	$\times 10^{-8}$	
v_9/v_{11}	6	6(2, 1A g)	000000001000B _{2u}	000000001000B _{2u}	2.036(12)	$\times 10^{-8}$	
v_9/v_{11}	6	6(4, 0A g)	000000001000B _{2u}	000000001000B _{2u}	-6.659(20)	$\times 10^{-8}$	
v_9/v_{11}	6	6(4, 1A g)	000000001000B _{2u}	000000001000B _{2u}	-4.958(25)	$\times 10^{-8}$	
v_9/v_{11}	6	6(4, 2A g)	000000001000B _{2u}	000000001000B _{2u}	-6.483(36)	$\times 10^{-9}$	
v_9/v_{11}	6	6(6, 0A g)	000000001000B _{2u}	000000001000B _{2u}	1.03858(63)	$\times 10^{-7}$	
v_9/v_{11}	6	6(6, 1A g)	000000001000B _{2u}	000000001000B _{2u}	2.264(10)	$\times 10^{-8}$	
v_9/v_{11}	6	6(6, 2A g)	000000001000B _{2u}	000000001000B _{2u}	-1.958(54)	$\times 10^{-9}$	
v_9/v_{11}	6	6(6, 3A g)	000000001000B _{2u}	000000001000B _{2u}	3.07(47)	$\times 10^{-11}$	
v_9/v_{11}	1	1(1, 0B _{3g})	000000001000B _{2u}	000000001000B _{1u}	7.67(11)	$\times 10^{-2}$	
v_9/v_{11}	2	2(2, 0B _{3g})	000000001000B _{2u}	000000001000B _{1u}	-7.9(1.6)	$\times 10^{-4}$	
v_9/v_{11}	3	3(1, 0B _{3g})	000000001000B _{2u}	000000001000B _{1u}	0.0		
v_9/v_{11}	3	3(3, 0B _{3g})	000000001000B _{2u}	000000001000B _{1u}	1.165(31)	$\times 10^{-4}$	
v_9/v_{11}	3	3(3, 1B _{3g})	000000001000B _{2u}	000000001000B _{1u}	1.82(19)	$\times 10^{-5}$	
v_9/v_{11}	4	4(2, 0B _{3g})	000000001000B _{2u}	000000001000B _{1u}	0.0		

Table A.1 (continued).

Polyad	Order	$\Omega(K, nC)$	$\{s\}$	C_1	$\{s'\}$	C_2	Value / cm ⁻¹
ν_9/ν_{11}	4	$4(4, 0B_3g)$	000000001000 B_{2u}	000000000010 B_{1u}			0.0
ν_9/ν_{11}	4	$4(4, 1B_3g)$	000000001000 B_{2u}	000000000010 B_{1u}			0.0
ν_9/ν_{11}	5	$5(1, 0B_3g)$	000000001000 B_{2u}	000000000010 B_{1u}			0.0
ν_9/ν_{11}	5	$5(3, 0B_3g)$	000000001000 B_{2u}	000000000010 B_{1u}			0.0
ν_9/ν_{11}	5	$5(3, 1B_3g)$	000000001000 B_{2u}	000000000010 B_{1u}			0.0
ν_9/ν_{11}	5	$5(5, 0B_3g)$	000000001000 B_{2u}	000000000010 B_{1u}			0.0
ν_9/ν_{11}	5	$5(5, 1B_3g)$	000000001000 B_{2u}	000000000010 B_{1u}			0.0
ν_9/ν_{11}	5	$5(5, 2B_3g)$	000000001000 B_{2u}	000000000010 B_{1u}			0.0
ν_9/ν_{11}	6	$6(2, 0B_3g)$	000000001000 B_{2u}	000000000010 B_{1u}			0.0
ν_9/ν_{11}	6	$6(4, 0B_3g)$	000000001000 B_{2u}	000000000010 B_{1u}			0.0
ν_9/ν_{11}	6	$6(4, 1B_3g)$	000000001000 B_{2u}	000000000010 B_{1u}			0.0
ν_9/ν_{11}	6	$6(6, 0B_3g)$	000000001000 B_{2u}	000000000010 B_{1u}			0.0
ν_9/ν_{11}	6	$6(6, 1B_3g)$	000000001000 B_{2u}	000000000010 B_{1u}			0.0
ν_9/ν_{11}	6	$6(6, 2B_3g)$	000000001000 B_{2u}	000000000010 B_{1u}			0.0
ν_9/ν_{11}	0	$0(0, 0A_g)$				2988.63465(16)	
ν_9/ν_{11}	2	$2(0, 0A_g)$	00000000010 B_{1u}	000000000010 B_{1u}	-3.1248(57)	$\times 10^{-3}$	
ν_9/ν_{11}	2	$2(2, 0A_g)$	00000000010 B_{1u}	000000000010 B_{1u}	-1.2727(26)	$\times 10^{-3}$	
ν_9/ν_{11}	2	$2(2, 1A_g)$	000000000010 B_{1u}	000000000010 B_{1u}	-6.148(33)	$\times 10^{-4}$	
ν_9/ν_{11}	4	$4(0, 0A_g)$	000000000010 B_{1u}	000000000010 B_{1u}	-8.649(49)	$\times 10^{-6}$	
ν_9/ν_{11}	4	$4(2, 0A_g)$	000000000010 B_{1u}	000000000010 B_{1u}	1.914(19)	$\times 10^{-6}$	
ν_9/ν_{11}	4	$4(2, 1A_g)$	000000000010 B_{1u}	000000000010 B_{1u}	-2.948(77)	$\times 10^{-6}$	
ν_9/ν_{11}	4	$4(4, 0A_g)$	000000000010 B_{1u}	000000000010 B_{1u}	-1.095(15)	$\times 10^{-6}$	
ν_9/ν_{11}	4	$4(4, 1A_g)$	000000000010 B_{1u}	000000000010 B_{1u}	4.55(11)	$\times 10^{-6}$	
ν_9/ν_{11}	4	$4(4, 2A_g)$	000000000010 B_{1u}	000000000010 B_{1u}	0.0		
ν_9/ν_{11}	6	$6(0, 0A_g)$	000000000010 B_{1u}	000000000010 B_{1u}	0.0		
ν_9/ν_{11}	6	$6(2, 0A_g)$	000000000010 B_{1u}	000000000010 B_{1u}	0.0		
ν_9/ν_{11}	6	$6(2, 1A_g)$	000000000010 B_{1u}	000000000010 B_{1u}	9.6906(36)	$\times 10^{-8}$	
ν_9/ν_{11}	6	$6(4, 0A_g)$	000000000010 B_{1u}	000000000010 B_{1u}	5.236(24)	$\times 10^{-9}$	
ν_9/ν_{11}	6	$6(4, 1A_g)$	000000000010 B_{1u}	000000000010 B_{1u}	-1.48639(52)	$\times 10^{-7}$	
ν_9/ν_{11}	6	$6(4, 2A_g)$	000000000010 B_{1u}	000000000010 B_{1u}	-4.759(12)	$\times 10^{-9}$	
ν_9/ν_{11}	6	$6(6, 0A_g)$	000000000010 B_{1u}	000000000010 B_{1u}	1.140(34)	$\times 10^{-9}$	
ν_9/ν_{11}	6	$6(6, 1A_g)$	000000000010 B_{1u}	000000000010 B_{1u}	-4.86(20)	$\times 10^{-10}$	
ν_9/ν_{11}	6	$6(6, 2A_g)$	000000000010 B_{1u}	000000000010 B_{1u}	3.94(18)	$\times 10^{-10}$	
ν_9/ν_{11}	6	$6(6, 3A_g)$	000000000010 B_{1u}	000000000010 B_{1u}	4.00(31)	$\times 10^{-11}$	
$\nu_5 + \nu_9/\nu_5 + \nu_{11}$	2	$0(0, 0A_g)$	000010001000 B_{1u}	000010001000 B_{1u}	-37.24178(27)		
$\nu_5 + \nu_9/\nu_5 + \nu_{11}$	4	$2(0, 0A_g)$	000010001000 B_{1u}	000010001000 B_{1u}	-1.210(28)	$\times 10^{-3}$	
$\nu_5 + \nu_9/\nu_5 + \nu_{11}$	4	$2(2, 0A_g)$	000010001000 B_{1u}	000010001000 B_{1u}	-4.674(84)	$\times 10^{-4}$	
$\nu_5 + \nu_9/\nu_5 + \nu_{11}$	4	$2(2, 1A_g)$	000010001000 B_{1u}	000010001000 B_{1u}	-1.121(17)	$\times 10^{-3}$	
$\nu_5 + \nu_9/\nu_5 + \nu_{11}$	6	$4(0, 0A_g)$	000010001000 B_{1u}	000010001000 B_{1u}	1.937(40)	$\times 10^{-5}$	
$\nu_5 + \nu_9/\nu_5 + \nu_{11}$	6	$4(2, 0A_g)$	000010001000 B_{1u}	000010001000 B_{1u}	-1.962(11)	$\times 10^{-5}$	
$\nu_5 + \nu_9/\nu_5 + \nu_{11}$	6	$4(2, 1A_g)$	000010001000 B_{1u}	000010001000 B_{1u}	-5.824(49)	$\times 10^{-5}$	
$\nu_5 + \nu_9/\nu_5 + \nu_{11}$	6	$4(4, 0A_g)$	000010001000 B_{1u}	000010001000 B_{1u}	1.2529(44)	$\times 10^{-5}$	
$\nu_5 + \nu_9/\nu_5 + \nu_{11}$	6	$4(4, 1A_g)$	000010001000 B_{1u}	000010001000 B_{1u}	9.046(69)	$\times 10^{-5}$	
$\nu_5 + \nu_9/\nu_5 + \nu_{11}$	6	$4(4, 2A_g)$	000010001000 B_{1u}	000010001000 B_{1u}	0.0		
$\nu_5 + \nu_9/\nu_5 + \nu_{11}$	3	$1(1, 0B_3g)$	000010001000 B_{1u}	000010000010 B_{2u}	-4.651(37)	$\times 10^{-1}$	
$\nu_5 + \nu_9/\nu_5 + \nu_{11}$	4	$2(2, 0B_3g)$	000010001000 B_{1u}	00001000000010 B_{2u}	4.207(20)	$\times 10^{-2}$	
$\nu_5 + \nu_9/\nu_5 + \nu_{11}$	5	$3(1, 0B_3g)$	000010001000 B_{1u}	00001000000010 B_{2u}	0.0		
$\nu_5 + \nu_9/\nu_5 + \nu_{11}$	5	$3(3, 0B_3g)$	000010001000 B_{1u}	00001000000010 B_{2u}	0.0		
$\nu_5 + \nu_9/\nu_5 + \nu_{11}$	5	$3(3, 1B_3g)$	000010001000 B_{1u}	00001000000010 B_{2u}	0.0		
$\nu_5 + \nu_9/\nu_5 + \nu_{11}$	6	$4(2, 0B_3g)$	000010001000 B_{1u}	00001000000010 B_{2u}	0.0		
$\nu_5 + \nu_9/\nu_5 + \nu_{11}$	6	$4(4, 0B_3g)$	000010001000 B_{1u}	00001000000010 B_{2u}	0.0		
$\nu_5 + \nu_9/\nu_5 + \nu_{11}$	6	$4(4, 1B_3g)$	000010001000 B_{1u}	00001000000010 B_{2u}	0.0		
$\nu_5 + \nu_9/\nu_5 + \nu_{11}$	2	$0(0, 0A_g)$	000010000010 B_{2u}	00001000000010 B_{2u}	-77.19664(26)		
$\nu_5 + \nu_9/\nu_5 + \nu_{11}$	4	$2(0, 0A_g)$	000010000010 B_{2u}	00001000000010 B_{2u}	1.772(23)	$\times 10^{-3}$	
$\nu_5 + \nu_9/\nu_5 + \nu_{11}$	4	$2(2, 0A_g)$	000010000010 B_{2u}	00001000000010 B_{2u}	-7.24(11)	$\times 10^{-4}$	
$\nu_5 + \nu_9/\nu_5 + \nu_{11}$	4	$2(2, 1A_g)$	000010000010 B_{2u}	00001000000010 B_{2u}	6.832(94)	$\times 10^{-4}$	
$\nu_5 + \nu_9/\nu_5 + \nu_{11}$	6	$4(0, 0A_g)$	000010000010 B_{2u}	00001000000010 B_{2u}	6.530(20)	$\times 10^{-5}$	
$\nu_5 + \nu_9/\nu_5 + \nu_{11}$	6	$4(2, 0A_g)$	000010000010 B_{2u}	00001000000010 B_{2u}	-2.0395(49)	$\times 10^{-5}$	
$\nu_5 + \nu_9/\nu_5 + \nu_{11}$	6	$4(2, 1A_g)$	000010000010 B_{2u}	00001000000010 B_{2u}	2.963(12)	$\times 10^{-5}$	
$\nu_5 + \nu_9/\nu_5 + \nu_{11}$	6	$4(4, 0A_g)$	000010000010 B_{2u}	00001000000010 B_{2u}	6.249(40)	$\times 10^{-6}$	
$\nu_5 + \nu_9/\nu_5 + \nu_{11}$	6	$4(4, 1A_g)$	000010000010 B_{2u}	00001000000010 B_{2u}	-4.996(17)	$\times 10^{-5}$	
$\nu_5 + \nu_9/\nu_5 + \nu_{11}$	6	$4(4, 2A_g)$	000010000010 B_{2u}	00001000000010 B_{2u}	0.0		

Appendix B. Comparision of polyad P_2 rovibrational levels with Reference [32]

The following tables (B.2 and B.3) compare the ν_9 and ν_{11} rovibrational levels measures by Sartakov *et al.* [32] with the present study, respectively.

Table B.2: Rovibrational energy levels of the ν_9 band from Ref. [32] compared to this work.

$\tilde{\nu}_{\text{obs}}/\text{cm}^{-1}$	Deviation $\Delta\tilde{\nu}/10^{-3}\text{ cm}^{-1}$		Assignment						
	Ref. [1]	This work	Ref. [1]	This work	J	K_a	K_c	C	α
3104.8862	3104.8788	-5.7		4.5	0	0	0	B_{2u}	1
3106.7100	3106.7028	-11.0		3.6	1	0	1	B_{3u}	2
3110.3525	3110.3458	-12.1		2.8	2	0	2	B_{2u}	2
3115.8023	3115.7958	-10.1		1.2	3	0	3	B_{3u}	3
3123.0415	3123.0350	-7.2		-2.5	4	0	4	B_{2u}	3
3155.2451	3155.2401	18.5		-44.0	7	0	7	B_{3u}	4
3169.3584	3169.4542	-6.3		0.8	8	0	8	B_{2u}	4
	3169.3513	—		11.5	13	—	—	B_{1u}	1 [†]
3185.0768	—	-3.2		—	9	0	9	B_{3u}	4
3110.7292	3110.7233	-2.2		1.2	1	1	0	B_{1u}	1
3114.5442	3114.5376	-2.5		-5.8	2	1	1	A_u	2
3120.2996	3120.2632	-4.3		-8.5	3	1	2	B_{1u}	2
3127.9209	3127.9167	-2.4		14.6	4	1	3	A_u	3
3110.5586	3110.5517	-1.2		1.4	1	1	1	A_u	2
3114.0361	3114.0294	-2.6		1.2	2	1	2	B_{1u}	3
3119.2490	3119.2426	-4.3		1.2	3	1	3	A_u	3
3126.1936	3126.1868	-3.0		0.7	4	1	4	B_{1u}	4
3126.1000	3126.0935	20.0		-4.4	2	2	0	B_{2u}	3
3131.5967	3131.5902	10.1		-4.8	3	2	1	B_{3u}	4
3138.9470	3138.9405	-4.1		-5.0	4	2	2	B_{2u}	4
3126.0943	3126.0935	19.5		-4.4	2	2	1	B_{3u}	3
3131.5685	3131.5619	11.5		-5.6	3	2	2	B_{2u}	3
3138.8630	3138.8570	2.3		-6.0	4	2	3	B_{3u}	3
3151.2309	3151.2280	11.1		-6.6	3	3	0	B_{1u}	3
3158.5540	3158.5475	4.0		1.1	4	3	1	A_u	4
3151.2309	3151.2278	12.3		-6.7	3	3	1	A_u	4
3158.5530	3158.5467	2.0		0.8	4	3	2	B_{1u}	5
3186.0435	3186.0374	-15.0		-3.8	4	4	0	B_{2u}	5
3186.0435	3186.0374	-15.0		-3.7	4	4	1	B_{3u}	4

[†] New assignment suggested for the 3169.35 cm^{-1} level.

Table B.3: Rovibrational energy levels of the ν_{11} band from Ref. [32] compared to this work.

Ref. [1]	$\tilde{\nu}_{\text{obs}} / \text{cm}^{-1}$		Deviation $\Delta\tilde{\nu}/10^{-3} \text{ cm}^{-1}$		Assignment				
	Ref. [1]	This work	Ref. [1]	This work	J	K_a	K_c	C	α
2988.6440	2988.6375	4.2		2.9	0	0	0	B_{1u}	1
2990.4705	2990.4644	3.3		2.9	1	0	1	A_u	1
2994.1174	2994.1118	2.6		2.8	2	0	2	B_{1u}	1
2999.5730	2999.5666	1.9		1.4	3	0	3	A_u	1
3006.8196	3006.8143	1.7		1.7	4	0	4	B_{1u}	1
2994.5019	2994.4954	1.7		1.9	1	1	0	B_{2u}	1
2998.3293	2998.3229	1.2		-0.6	2	1	1	B_{3u}	1
3004.0491	3004.0424	-0.3		-22.0	3	1	2	B_{2u}	1
3011.7212	3011.7150	-0.1		3.9	4	1	3	B_{3u}	1
2994.3264	2994.3202	3.0		3.2	1	1	1	B_{3u}	1
2997.8030	2997.7963	0.5		2.5	2	1	2	B_{2u}	1
3003.0142	3003.0078	-1.4		2.5	3	1	3	B_{3u}	1
3009.9558	3009.9492	0.1		2.2	4	1	4	B_{2u}	1
3009.9028	3009.8955	-4.6		1.1	2	2	0	B_{1u}	2
3015.4053	3015.3956	-4.0		-2.2	3	2	1	A_u	2
3022.7644	3022.7583	0.8		0.5	4	2	2	B_{1u}	2
3009.8967	3009.8928	-6.7		4.2	2	2	1	A_u	1
3015.3757	3015.3636	-5.1		-4.7	3	2	2	B_{1u}	1
3022.6763	3022.6694	-0.7		-0.3	4	2	3	A_u	1
3035.0911	3035.0828	-4.3		-0.6	3	3	0	B_{2u}	2
3042.4075	3042.4026	-0.3		1.4	4	3	1	B_{3u}	2
3035.0911	3035.0829	-3.1		-0.4	3	3	1	B_{3u}	2
3042.4067	3042.3993	1.0		-1.0	4	3	2	B_{2u}	2
3069.9812	—	4.3		—	4	4	0	B_{1u}	3
3069.9812	3069.9721	4.3		-3.2	4	4	1	A_u	2

References

- [1] Cape, JN. Effects of airborne volatile organic compounds on plants. *Environ Pollut* 2003;122:145–157.
- [2] Munné-Bosch, S, Peñuelas, J, Asensio, D, Llusià, J. Airborne ethylene may alter antioxidant protection and reduce tolerance of holm oak to heat and drought stress. *Plant Physiol* 2004;136:2937–2947.
- [3] Romani, PN, Jennings, DE, Bjoraker, GL, Sada, PV, McCabe, GH, Boyle, RJ. Temporally varying ethylene emission on Jupiter. *Icarus* 2008;198:420–434.
- [4] Kostiuk, T, Romani, P, Espenak, F, Livengood, T, Goldstein, J. Temperature and abundances in the jovian auroral stratosphere. 2. Ethylene as a probe of the microbar region. *J Geophys Res* 1993;98:18823–18830.

- [5] Griffith, C, Bézard, B, Greathouse, T, Kelly, D, Lacy, J, Noll, K. Thermal infrared imaging spectroscopy of Shoemaker-Levy 9 impact sites: Spatial and vertical distributions of NH₃, C₂H₄, and 10 μm dust emission. *Icarus* 1997;128:275–293.
- [6] Bézard, B, Moses, J, Lacy, J, Greathouse, T, Richter, M, Griffith, C. Detection of Ethylene (C₂H₄) on Jupiter and Saturn in Non-Auroral Regions. *Bull Am Astron Soc* 2001;33:1079.
- [7] Schulz, B, Encrénaz, T, Bézard, B, Romani, P, Lellouch, E, Atreya, S. Detection of C₂H₄ in Neptune from ISO/PHT-S observations. *Astron Astrophys* 1999;350:L13–L17.
- [8] Encrénaz, T. ISO observations of planetary atmospheres. *Adv Space Res* 2002;30:1967–1970.
- [9] Roe, H, de Pater, I, McKay, C. Seasonal variation of Titan’s stratospheric ethylene (C₂H₄) observed. *Icarus* 2004;169:440–461.
- [10] Jr, RV, Sandel, B, Strobel, D. New perspectives on Titan’s upper atmosphere from a reanalysis of the Voyager 1 UVS solar occultations . *Icarus* 2004;170:91–112.
- [11] Coustenis, A, Achterberg, RK, Conrath, BJ, Jennings, DE, Marten, A, Gautier, D, et al. The composition of Titan’s stratosphere from Cassini/CIRS mid-infrared spectra. *Icarus* 2007;189(35–62).
- [12] Sawada, S, Totsuka, T. Natural and anthropogenic sources and fate of atmospheric ethylene. *Atmospheric Environment* 1986;20(5):821–832.
- [13] Duncan, J, Ferguson, A. Local mode and normal mode interpretations of the ch and cd stretching vibrational manifolds in C₂H₄ and C₂D₄. *J Chem Phys* 1988;89(7):4216–4226.
- [14] Bach, M, Georges, R, Herman, M, Perrin, A. Investigation of the fine structure in overtone absorption bands of ¹²C₂H₄. *Mol Phys* 1999;97(1):265–277.
- [15] Platz, P, Demtröder, W. Sub-doppler optothermal overtone spectroscopy of ethylene and dichloroethylene. *Chem Phys Lett* 1998;294(4–5):397–405.
- [16] Rossi, A, Buffa, R, Scotony, M, Bassi, D, Iannotta, S, Boschetti, A. Optical enhancement of diode laser-photoacoustic trace gas detection by means of external Fabry-Perot cavity. *Appl Phys Lett* 2005;87:041110.
- [17] Parkes, A, Lindley, R, Orr-Ewing, A. Absorption cross-sections and pressure broadening of rotational lines in the ν₅ + ν₉ band of ethene measured by diode laser cavity ring down spectroscopy. *Phys Chem Chem Phys* 2004;6:5313–5317.

- [18] Kapitanov, V, Ponomarev, Y. High resolution ethylene absorption spectrum between 6035 and 6210 cm⁻¹. *Appl Phys B* 2008;90:235–241.
- [19] Boschetti, A, Bassi, D, Iacob, E, Iannotta, S, Ricci, L, Scotoni, M. Resonant photoacoustic simultaneous detection of methane and ethylene by means of a 1.63 μm diode laser. *Appl Phys* 2002;74(3):273–278.
- [20] Rothman, LS, Jacquemart, D, Barbe, A, Benner, DC, Birk, M, Brown, LR, et al. The HITRAN 2004 molecular spectroscopic database. *J Quant Spectrosc Radiat Transfer* 2005;96:139–204.
- [21] Margolis, J. Measured line positions and strengths of methane between 5500 and 6180 cm⁻¹. *Appl Opt* 1988;27(19):4038–4051.
- [22] Bach, M, Georges, R, Hepp, M, Herman, M. Slit-jet Fourier transform infrared spectroscopy in ¹²C₂H₄: Cold and hot bands near 3000 cm⁻¹. *Chem Phys Lett* 1998;294:533–537.
- [23] Foster, RB, Hills, GW, Jones, WJ. Raman spectra of asymmetric top molecules. Part V. – The ν₁, ν₃ and ν₅ bands of ethylene. *Mol Phys* 1977;33(1589–1610).
- [24] Rothman, L, Gamache, R, Tipping, R, Rinsland, C, Smith, M, Benner, D, et al. The HITRAN molecular database – Editions of 1991 and 1992. *J Quant Spectrosc Radiat Transfer* 1992;48(5–6):469–507.
- [25] Georges, R, Bach, M, Herman, M. High resolution FTIR spectroscopy using a slit jet: Sampling the overtone spectrum of ¹²C₂H₄. *Mol Phys* 1997;90(3):381–387.
- [26] Kapitanov, V, Ponomarev, Y, Tyryshkin, I, Rostov, A. Dual-channel opto-acoustic diode laser spectrometer and fine structure of methane absorption spectra in 6070–6180 cm⁻¹ region. *Spectrochimica Acta Part A* 2007;66(45):811–818.
- [27] <http://www.scitec.uk.com>.
- [28] <http://www.nsu.ru/srd/l1s/english/angstrom.htm>.
- [29] <http://spectra.iao.ru/>.
- [30] Herzberg, G. Infrared and Raman spectra of polyatomic molecules. New York: D. Van Nostrand Company Inc.; 1945.
- [31] Raballand, W, Rotger, M, Boudon, V, Loëte, M. Spectroscopy of X₂Y₄ (*D*₂*h*) molecules : Tensorial formalism adapted to the *O*(3) ⊃ *D*₂*h* chain, Hamiltonian and transition moment operators. *J Mol Spectrosc* 2003;217:239–248.

- [32] Sartakov, B, Oomens, J, Reuss, J, Fayt, A. Interaction of vibrational fundamental and combination states of ethylene in the 3 μm region. *J Mol Spectrosc* 1997;185:31–47.
- [33] Wenger, C, Boudon, V, Champion, JP, Pierre, G. Highly-Spherical Top Data System (HTDS) software for the spectrum simulation of octahedral XY_6 molecules. *J Quant Spectrosc Radiat Transfer* 2000;66(1):1–16.
- [34] Champion, JP, Loëte, M, Pierre, G. Spherical top spectra. In: Rao, KN, Weber, A, editors. *Spectroscopy of the Earth's atmosphere and interstellar medium*. San Diego: Academic Press; 1992, p. 339–422.
- [35] Cheblal, N, Loëte, M, Boudon, V. Development of the dipole moment and polarizability operators of octahedral molecules. *J Mol Spectrosc* 1999;197:222–231.
- [36] Boudon, V, Champion, JP, Gabard, T, Loëte, M, Michelot, F, Pierre, G, et al. Symmetry-adapted tensorial formalism to model rovibrational and rovibronic spectra of molecules pertaining to various point groups. *J Mol Spectrosc* 2004;228:620–634.
- [37] Wenger, C, Raballand, W, Rotger, M, Boudon, V. D_{2h} top data system (D_{2h} TDS) software for spectrum simulation of X_2Y_4 asymmetric molecules. *J Quant Spectrosc Radiat Transfer* 2005;95:521–538.
- [38] <http://icb.u-bourgogne.fr/OMR/SMA/SHTDS>.
- [39] Wenger, C, Boudon, V, Rotger, M, Sanzharov, M, Champion, JP. XTDS and SPVIEW: Graphical tools for the analysis and simulation of high-resolution molecular spectra. *J Mol Spectrosc* 2008;251(1-2):102–113.
- [40] Boudon, V, Rotger, M, Zvereva-Loëte, N, Loëte, M. The SO_2F_2 quasi-spherical top: Correspondance between tensorial and Watson's formalisms. *J Mol Struct* 2006;780–781:124–133.
- [41] Papoušek, D, Aliev, M. Molecular vibrational-rotational spectra. New York: Elsevier; 1982.
- [42] Bach, M, Georges, R, Herman, M, Perrin, A. Investigation of the fine structure in overtone absorption bands of $^{12}\text{C}_2\text{H}_4$. *Mol Phys* 1999;97:265–277.
- [43] Willaert, F, Demaison, J, Margulès, L, Mäder, H, Spahn, H, Giessen, T, et al. The spectrum of ethylene from microwave to submillimeter-wave. *Mol Phys* 2006;104:273–292.
- [44] Ooomens, J, Reuss, J, Mellau, GC, Klee, S, Gulaczyk, I, Fayt, A. The ethylene hot band spectrum near 3000 cm^{-1} . *J Mol Spectrosc* 1996;180:236–248.